Inorg. Chem. **2003**, *42*, 3016–3025

Synthesis and Characterization of Reduced Heme and Heme/Copper Carbonmonoxy Species

Ryan M. Kretzer, Reza A. Ghiladi, Estelle L. Lebeau, Hong-Chang Liang, and Kenneth D. Karlin*

Department of Chemistry, The Johns Hopkins University, Charles and 34th Streets, Baltimore, Maryland 21218

Received August 22, 2002

Carbon monoxide readily binds to heme and copper proteins, acting as a competitive inhibitor of dioxygen. As such, CO serves as a probe of protein metal active sites. In our ongoing efforts to mimic the active site of cytochrome *c* oxidase, reactivity toward carbon monoxide offers a unique opportunity to gain insight into the binding and spectroscopic characteristics of synthetic model compounds. In this paper, we report the synthesis and characterization of CO-adducts of ($^{5/6}$L)Fe^{II}, [($^{5/6}$L)Fe^{II}···Cu^{I}](B(C$_6$F$_5$)$_4$), and [(TMPA)Cu^{I}(CH$_3$CN)](B(C$_6$F$_5$)$_4$), where TMPA = tris(2-pyridylmethyl)amine and $^{5/6}$L = a tetraarylporphyrinate tethered in either the 5-position (^{5}L) or 6-position (^{6}L) to a TMPA copper binding moiety. Reaction of ($^{5/6}$L)Fe^{II} {in THF (293 K): UV–vis 424 (Soret), 543–544 nm; ^{1}H NMR $\delta_{pyrrole}$ 52–59 ppm (4 peaks); ^{2}H NMR (from (^{5}L-d_8)Fe^{II}) $\delta_{pyrrole}$ 53.3, 54.5, 55.8, 56.4 ppm} with CO in solution at RT yielded ($^{5/6}$L)Fe^{II}–CO {in THF (293 K): UV–vis 413–414 (Soret), 532–533 nm; IR ν(CO)$_{Fe}$ 1976–1978 cm^{-1}; ^{1}H NMR $\delta_{pyrrole}$ 8.8 ppm; ^{2}H NMR (from (^{5}L-d_8)Fe^{II}–CO) $\delta_{pyrrole}$ 8.9 ppm; ^{13}C NMR $\delta_{(CO)Fe}$ 206.8–207.1 ppm (2 peaks)}. Experiments repeated in acetonitrile, acetone, toluene, and dichloromethane showed similar spectroscopic data. Binding of CO resulted in a change from five-coordinate, high-spin Fe(II) to six-coordinate, low-spin Fe(II), as evidenced by the upfield shift of the pyrrole resonances to the diamagnetic region (^{1}H and ^{2}H NMR spectra). Addition of CO to [($^{5/6}$L)Fe^{II}···Cu^{I}](B(C$_6$F$_5$)$_4$) {in THF (293 K): UV–vis (^{6}L only) 424 (Soret), 546 nm; ^{1}H NMR $\delta_{pyrrole}$ 54–59 ppm (multiple peaks); ^{2}H NMR (from [(^{5}L-d_8)Fe^{II}···Cu^{I}](B(C$_6$F$_5$)$_4$)) $\delta_{pyrrole}$ 53.4 ppm (br)} gave the bis-carbonyl adduct [($^{5/6}$L)Fe^{II}–CO···Cu^{I}–CO](B(C$_6$F$_5$)$_4$) {in THF (293 K): UV–vis (^{6}L only) 413 (Soret), 532 nm; IR ν(CO)$_{Fe}$ 1971–1973 cm^{-1}, ν(CO)$_{Cu}$ 2091–2093 cm^{-1}, ∼2070(sh) cm^{-1}; ^{1}H NMR $\delta_{pyrrole}$ 8.7–8.9 ppm; ^{2}H NMR (from [(^{5}L-d_8)Fe^{II}–CO···Cu^{I}–CO](B(C$_6$F$_5$)$_4$)) $\delta_{pyrrole}$ 8.9 ppm; ^{13}C NMR $\delta_{(CO)Fe}$ 206.8–208.1 ppm (2 peaks), $\delta_{(CO)Cu}$ 172.4 (^{5}L), 178.2 (^{6}L) ppm}. Experiments in acetonitrile, acetone, and toluene exhibited spectral features similar to those reported. The [($^{5/6}$L)Fe^{II}–CO···Cu^{I}–CO](B(C$_6$F$_5$)$_4$) compounds yielded (CO)$_{Fe}$ spectra analogous to those seen for ($^{5/6}$L)Fe^{II}–CO and (CO)$_{Cu}$ spectra similar to those seen for [(TMPA)Cu^{I}–CO](B(C$_6$F$_5$)$_4$) {in THF (293 K): IR ν(CO)$_{Cu}$ 2091 cm^{-1}, ∼2070(sh) cm^{-1}; ^{13}C NMR $\delta_{(CO)Cu}$ 180.3 ppm}. Additional IR studies were performed in which the [(^{5}L)Fe^{II}–CO···Cu^{I}–CO](B(C$_6$F$_5$)$_4$) in solution was bubbled with argon in an attempt to generate the iron-only mono-carbonyl [(^{5}L)Fe^{II}–CO···Cu^{I}](B(C$_6$F$_5$)$_4$) species; in coordinating solvent or with axial base present, decreases in characteristic IR-band intensities revealed complete loss of CO from copper and variable loss of CO from the heme.

Introduction

Carbon monoxide binding to hemes and hemoproteins has always been a subject of great interest, especially as a probe or surrogate for dioxygen (O_2) binding to iron-porphyrin centers.[1−3] Thus, especially for the O_2-carriers hemoglobin and myoglobin, CO has been employed to obtain structural insights and used as a dynamic probe of the active site through fast time scale investigations of the photochemical ejection and subsequent rebinding of CO.[3−8] Other examples

* To whom correspondence should be addressed. E-mail: karlin@jhu.edu.

(1) Ghosh, A. In *The Porphyrin Handbook*; Kadish, K. M., Smith, K. M., Guilard, R., Eds.; Academic Press: San Diego, CA, 2000; Vol. 7.
(2) Spiro, T. G.; Zgierski, M. Z.; Kozlowski, P. M. *Coord. Chem. Rev.* **2001**, *219−221*, 923−936.
(3) Spiro, T. G.; Kozlowski, P. M. *Acc. Chem. Res.* **2001**, *34*, 137−144.
(4) Uchida, T. I., H.; Ishimori, K.; Morishima, I.; Nakajima, H.; Aono, S.; Mizutani, Y.; Kitagawa, T. *Biochemistry* **2000**, *39*, 12747−12752.

10.1021/ic020521i CCC: $25.00
Published on Web 03/29/2003

delineating the importance of carbon monoxide can be found in several biologically important systems or processes. The enzyme heme-oxygenase (HO) breaks down heme forming biliverdin and CO, thereby providing the means for removing damaged (i.e., toxic) heme.[9−12] The heme-protein sensor CooA mediates transcriptional and regulatory events upon binding of CO to its unique heme prosthetic group; this and other heme sensors of small molecules (i.e., CO, O_2, and NO) have elicited excitement and further investigation into newer types of heme proteins.[13,14] Further, there is also the suggestion that CO itself can act as a physiological effector.[15−18]

Our own interest in carbon monoxide chemistry arises from our general program in synthetic modeling of the active site of cytochrome *c* oxidase (C*c*O),[19−25] the terminal respiratory enzyme for aerobic organisms responsible for the $4e^-/4H^+$ reduction of O_2 to water occurring at a heme-copper heterobinuclear active site; protein X-ray structures are now available.[26,27] Carbon monoxide bound to the heme of the heme-Cu active site has been a very important protein derivative in the elucidation of the C*c*O O_2-binding and reduction mechanism.[28−32] Flash photolysis of the photolabile

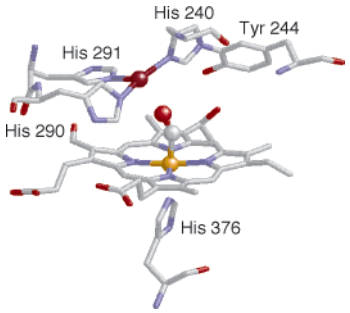

Figure 1. Crystal structure of the carbon monoxide adduct of cytochrome *c* oxidase. Coordinates (1OCO) were taken from the Protein Data Bank (Brookhaven) and displayed using the program Rasmol.

Chart 1

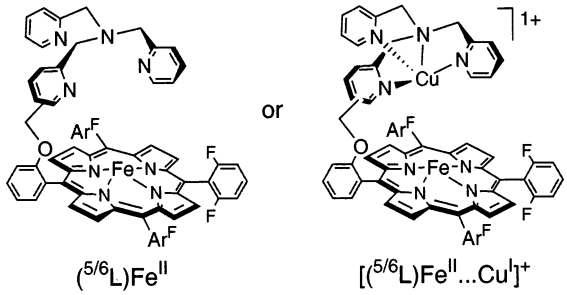

CO-adduct has been used as an active site probe, in fact showing that the CO switches transiently to the nearby (∼ 4.5 Å away) Cu_B.[33−35] A crystal structure of the heme-CO adduct of cytochrome *c* oxidase has also been reported (Figure 1).[26]

Considerable efforts in our modeling studies have focused on the binucleating ligands ^{5}L and ^{6}L, wherein a tetradentate derivatized TMPA moiety {TMPA = tris(2-pyridylmethyl)-amine} is tethered to the periphery of a tetraarylporphyrinate through one pyridyl group of TMPA, either in the 5-position (^{5}L) or 6-position (^{6}L) (Chart 1).[24,25,36−38] Utilizing these ligands, we described μ-oxo complexes $[(^{5/6}L)Fe^{III}-O-Cu^{II}]^+$, formed from O_2-reactions with reduced precursors $[(^{5/6}L)Fe^{II}\cdots Cu^{I}]^+$;[24,25] analogous chemistry occurs with separate (untethered) heme and copper complexes, forming $[(F_8TPP)Fe^{III}-O-Cu^{II}(TMPA)]^+$ {F_8TPP = tetrakis(2,6-difluorophenyl)porphyrinate(2−)}.[19] In fact, recent work has

(5) Chu, K. V. J.; McMahon, B. H.; Sweet, R. M.; Berendzen, J.; Schlichting, I. *Nature* **2000**, *403*, 921−923.
(6) Taube, D.; Traylor, T. G.; Magde, D.; Walda, K.; Luo, J. *J. Am. Chem. Soc.* **1992**, *114*, 9182−9188.
(7) Greenwood, C.; Gibson, Q. H. *J. Biol. Chem.* **1967**, *242*, 1782−1787.
(8) Greenwood, C.; Gibson, Q. H. *Biochem. J.* **1963**, *86*, 541−554.
(9) Sono, M.; Roach, M. P.; Coulter, E. D.; Dawson, J. H. *Chem. Rev.* **1996**, *96*, 2841−2887.
(10) Ortiz de Montellano, P. R.; Wilks, A. *Adv. Inorg. Chem.* **2001**, *51*, 359−407.
(11) Ortiz de Montellano, P. R. *Curr. Opin. Chem. Biol.* **2000**, *4*, 221−227.
(12) Fujii, H.; Zhang, Y.; Tomita, T.; Ikeda-Saito, M.; Yoshida, T. *J. Am. Chem. Soc.* **2001**, *123*, 6475−6484.
(13) Jain, R.; Chan, M. K. *J. Biol. Inorg. Chem., JBIC* **2003**, *8*, 1−11.
(14) Rodgers, K. R. *Curr. Opin. Chem. Biol.* **1999**, *3*, 158−167.
(15) Verma, A.; Hirsch, D. J.; Glatt, C. E.; Ronnett, G. V.; Snyder, S. H. *Science* **1993**, *259*, 381−384.
(16) Snyder, S. H.; Jaffrey, S. R.; Zakhary, R. *Brain Res. Rev.* **1998**, *26*, 167−175.
(17) Dore, S.; Goto, S.; Sampei, K.; Blackshaw, S.; Hester, L. D.; Ingi, T.; Sawa, A.; Traystman, R. J.; Koehler, R. C.; Snyder, S. H. *Neuroscience* **2000**, *99*, 587−592.
(18) Cary, S. P. L.; Marletta, M. A. *J. Clin. Invest.* **2001**, *107*, 1071−1073.
(19) Ghiladi, R. A.; Hatwell, K. R.; Karlin, K. D.; Huang, H.-w.; Moënne-Loccoz, P.; Krebs, C.; Huynh, B. J.; Marzilli, L. A.; Cotter, R. J.; Kaderli, S.; Zuberbühler, A. D. *J. Am. Chem. Soc.* **2001**, *123*, 6183−6184.
(20) Ghiladi, R. A.; Kretzer, R. M.; Guzei, I.; Rheingold, A. L.; Neuhold, Y.-M.; Hatwell, K. R.; Zuberbühler, A. D.; Karlin, K. D. *Inorg. Chem.* **2001**, *40*, 5754−5767.
(21) Kopf, M.-A.; Karlin, K. D. In *Biomimetic Oxidations*; Meunier, B., Ed.; Imperial College Press: London, 2000; Chapter 7, pp 309−362.
(22) Kopf, M.-A.; Neuhold, Y.-M.; Zuberbühler, A. D.; Karlin, K. D. *Inorg. Chem.* **1999**, *38*, 3093−3102.
(23) Kopf, M.-A.; Karlin, K. D. *Inorg. Chem.* **1999**, *38*, 4922−4923.
(24) Ghiladi, R. A.; Ju, T. D.; Lee, D.-H.; Moënne-Loccoz, P.; Kaderli, S.; Neuhold, Y.-M.; Zuberbühler, A. D.; Woods, A. S.; Cotter, R. J.; Karlin, K. D. *J. Am. Chem. Soc.* **1999**, *121*, 9885−9886.
(25) Ju, T. D.; Ghiladi, R. A.; Lee, D.-H.; van Strijdonck, G. P. F.; Woods, A. S.; Cotter, R. J.; Young, J., V. G.; Karlin, K. D. *Inorg. Chem.* **1999**, *38*, 2244−2245.
(26) Yoshikawa, S.; Shinzawa-Itoh, K.; Nakashima, R.; Yaono, R.; Yamashita, E.; Inoue, N.; Yao, M.; Jei-Fei, M.; Libeu, C. P.; Mizushima, T.; Yamaguchi, H.; Tomizaki, T.; Tsukihara, T. *Science* **1998**, *280*, 1723−1729.
(27) Michel, H.; Behr, J.; Harrenga, A.; Kannt, A. *Annu. Rev. Biophys. Biomol. Struct.* **1998**, *27*, 329−356.
(28) Babcock, G. T. *Proc. Natl. Acad. Sci. U.S.A.* **1999**, *96*, 12971−12973.
(29) Kitagawa, T.; Ogura, T. *Prog. Inorg. Chem.* **1997**, *45*, 431−479.
(30) Szundi, I.; Liao, G.-L.; Einarsdottir, O. *Biochemistry* **2001**, *40*, 2332−2339.
(31) Han, S.; Takahashi, S.; Rousseau, D. L. *J. Biol. Chem.* **2000**, *275*, 1910−1919.
(32) Giuffre, A.; Forte, E.; Antonini, G.; D'Itri, E.; Brunori, M.; Soulimane, T.; Buse, G. *Biochemistry* **1999**, *38*, 1057−1065.
(33) Woodruff, W. H. *J. Bioenerg. Biomembr.* **1993**, *25*, 177−188.
(34) Einarsdottir, O.; Dyer, R. L.; Lemon, D. D.; Killough, P. M.; Hubig, S. M.; Atherton, S. J.; Lopez-Garriga, J. J.; Palmer, G.; Woodruff, W. H. *Biochemistry* **1993**, *32*, 12013−12024.
(35) Koutsoupakis, K.; Stafrakis, S.; Pinakoulaki, E.; Soulimane, T.; Varotsis, C. *J. Biol. Chem.* **2002**, *277*, 32860−32866.
(36) Obias, H. V.; van Strijdonck, G. P. F.; Lee, D.-H.; Ralle, M.; Blackburn, N. J.; Karlin, K. D. *J. Am. Chem. Soc.* **1998**, *120*, 9696−9697.
(37) Ju, T. D.; Woods, A. S.; Cotter, R. J.; Moënne-Loccoz, P.; Karlin, K. D. *Inorg. Chim. Acta* **2000**, *297*, 362−372.
(38) Moënne-Loccoz, P.; Richter, O.-M. H.; Huang, H.-w.; Wasser, I. M.; Ghiladi, R. A.; Karlin, K. D.; de Vries, S. *J. Am. Chem. Soc.* **2000**, *122*, 9344−9345.

shown that O_2-adducts of the ^{6}L or untethered systems can best be described as peroxo species, $[(^6L)Fe^{III}-(O_2^{2-})-Cu^{II}]^+$ [24] or $[(F_8TPP)Fe^{III}-(O_2^{2-})-Cu^{II}(TMPA)]^+$,[19] respectively. To expand and broaden the scope of this work, we describe here the CO-binding chemistry of heme(empty-tether) $(^{5/6}L)Fe^{II}$ and heme-copper $[(^{5/6}L)Fe^{II}\cdots Cu^{I}](B(C_6F_5)_4)$ complexes (see Chart 1). Bis-carbonyl (i.e., Fe−CO···Cu−CO) or mono-carbonyl (heme-CO only) adducts were formed and characterized using a variety of probes, including UV−vis, infrared (IR), and multinuclear (i.e., ^{1}H, ^{2}H and ^{13}C) magnetic resonance spectroscopies. The importance of this area is reflected by the recently published complementary study by Collman and co-workers[39] on carbon monoxide binding to synthetic trisimidazole-copper picket metalloporphyrins.

Experimental Section

Materials and Methods. All reagents and solvents were purchased from commercial sources and were of reagent quality unless otherwise stated. Air-sensitive compounds were handled under argon atmosphere using standard Schlenk techniques, or in an MBraun Labmaster 130 inert atmosphere (<1 ppm O_2, <1 ppm H_2O) glovebox filled with nitrogen. Acetonitrile (CH_3CN), methylene chloride (CH_2Cl_2), and heptane were distilled from calcium hydride, tetrahydrofuran and toluene from sodium/benzophenone, and acetone from Drierite (97% $CaSO_4$, 3% $CoCl_2$) all under argon. Deoxygenation of these solvents was achieved by bubbling with argon for 30 min followed by 3 freeze/pump/thaw cycles prior to introduction into the glovebox. NMR solvents were distilled as described here and deoxygenated through 5 freeze/pump/thaw cycles. Addition of carbon monoxide (Matheson Gas Products) for UV−vis, IR, ^{1}H NMR, and ^{2}H NMR spectroscopic studies was effected by direct bubbling through an R & D Separations oxygen/moisture trap model OT3-4 into the sample solution via a syringe needle. Electrospray ionization (ESI-MS) mass spectra were recorded on a Finnigan LCQ ion trap mass spectrometer (San Jose, CA) equipped with a standard electrospray source. ^{13}CO was purchased in 100 mL breakseals from ICON Services, Inc., Marion, NY.

Synthesis. $(F_8TPP)Fe^{II}$,[20,22] $(F_8TPP\text{-}d_8)Fe^{II}$,[20,22] $(^5L)Fe^{II}$,[25] $(^6L)Fe^{II}$,[25,40] $(^6L\text{-}d_8)Fe^{II}$,[40] $[(^6L)Fe^{II}\cdots Cu^{I}](B(C_6F_5)_4)$,[40] $[(^6L\text{-}d_8)Fe^{II}\cdots Cu^{I}](B(C_6F_5)_4)$,[40] and $[Cu^{I}(CH_3CN)_4](B(C_6F_5)_4)$[41] were synthesized according to published procedures.

$[(TMPA)Cu^{I}(CH_3CN)](B(C_6F_5)_4)$. Under an Ar atmosphere in a standard 100 mL Schlenk flask was added the off-white solid TMPA[42] (110 mg, 0.380 mmol) and 25 mL degassed diethyl ether. To the resulting light yellow solution was added 1 equiv of $[Cu^{I}(CH_3CN)_4](B(C_6F_5)_4)$ (343 mg, 0.378 mmol) under Ar. The now light orange solution was stirred for 15 min, followed by the slow addition of a large excess (~50 mL) of degassed pentane over the course of 10 min. The flask was cooled to −20 °C for 2 h, after which an oily, yellow precipitate had formed. After decantation, the yellow precipitate was dried in vacuo overnight to yield 318 mg (81.3%) of yellow solid: ^{1}H NMR (400 MHz, THF-d_8, 293 K) 8.76 (br, 3 H), 7.86 (m, 3 H), 7.50 (br, 6 H), 4.29 (v br, 6 H), 2.05 (s, CH_3CN). Anal. Calcd for $[(TMPA)Cu^{I}(CH_3CN)](B(C_6F_5)_4$ $C_{44}H_{21}BCuF_{20}N_5$: C, 49.21; H, 1.97; N, 6.52. Found: C, 48.90; H, 1.97; N, 6.42.

$(^5L\text{-}d_8)Fe^{II}$. This complex was synthesized in an analogous procedure to that previously reported for $(^6L\text{-}d_8)Fe^{II}$.[40] UV−vis (nm, THF, 293 K) 424 (Soret), 543; ^{2}H NMR (61.3 MHz, THF, 293 K) 53.3, 54.5, 55.8, 56.4 ppm (pyrr H).

$[(^5L)Fe^{II}\cdots Cu^{I}](B(C_6F_5)_4)$. In the glovebox, in a 50 mL Schlenk flask were dissolved $(^5L)Fe^{II}$ (120 mg, 0.11 mmol) and $[Cu^{I}(CH_3CN)_4](B(C_6F_5)_4)$ (100 mg, 0.11 mmol, 1 equiv) in ~2−3 mL deaerated THF. After allowing the deep red solution to stir for 15 min, 10−15 mL deaerated heptane (5:1 v/v) was added, thereby forming an opaque precipitate. The mother liquor was removed by decantation and the solid washed with fresh, deaerated heptane. After the residual solvent was removed under vacuum for 45 min on the benchtop, the flask with resulting solid was reintroduced into the glovebox. $[(^5L)Fe^{II}\cdots Cu^{I}](B(C_6F_5)_4)$ was thus obtained in high yield as a deep red/purple microcrystalline solid. The purity was judged to be suitable based on ^{1}H NMR spectroscopy (lack of Fe^{III}−OH impurities at $\delta = 80-82$ ppm) and mass spectrometry. UV−vis (nm, toluene, 293 K) 413, 432(sh) (Soret), 530, 556(sh); ^{1}H NMR (400 MHz, THF-d_8, 293 K) 58.8 (s, sh, pyrr H), 57.7 (s, sh, pyrr H), 54.7 (s, sh, pyrr H), 54.0 (s, sh, pyrr H), ca. 9.0 (s, br), 8.31 (s, sh), 7.4−8.0 (mult peaks, br, pyridyl H), 7.25 (s, sh), 6.80 (s, sh), 6.41 (s, sh), 5.77 (d, $J = 56.8$ Hz), 5.10 (s, sh), 4.73 (s, sh), 4.28 (s, sh), ca. 2.6 (s, br). ESI-MS Found: 1157.5 {m/z [M − $(B(C_6F_5)_4)^-$]$^+$}. Calcd: 1158.4.

$[(^5L\text{-}d_8)Fe^{II}\cdots Cu^{I}](B(C_6F_5)_4)$. In a glovebox, $(^5L\text{-}d_8)Fe^{II}$ (20 mg, 0.018 mmol) and $[Cu^{I}(CH_3CN)_4](B(C_6F_5)_4)$ (17 mg, 0.019 mmol) were dissolved in 1 mL of THF and allowed to stir for 5 min, thereby forming $[(^5L\text{-}d_8)Fe^{II}\cdots Cu^{I}](B(C_6F_5)_4)$ in situ. This deep red solution was then transferred to an airtight, screw-cap NMR tube. ^{2}H NMR (61.3 MHz, THF, 293 K) 53.4 ppm (s, br, pyrr H).

UV−Vis Spectroscopy. Absorption spectra were obtained at room temperature using either a Shimadzu UV 160U or a Hewlett-Packard model 8453 diode array spectrophotometer operating HP Chemstation software. Each sample was prepared in an air-free cuvette assembly in which a 10 mm quartz cuvette was fused to a glass tube that was equipped with a high-vacuum stopcock and a 14/20 ground glass joint as described elsewhere.[43,44] In a drybox, solid $(^{5/6}L)Fe^{II}$ or $[(^{5/6}L)Fe^{II}\cdots Cu^{I}]$ $(B(C_6F_5)_4)$ was dissolved in one of the organic solvents chosen for these studies. On the benchtop, carbonylation was effected by puncturing the rubber septum of the cuvette assembly with a long needle, followed by direct bubbling of CO through the sample solution for ~10 s. For each solvent, two samples were prepared in separate cuvettes, the first at a concentration at which the Soret band fell between 0.5 and 1 absorbance units and the second at a concentration where the α band fell in this absorbance range. Extinction coefficients (M^{-1} cm^{-1}) were determined as the average of at least two trials. All wavelengths are reported in nanometers.

Infrared Spectroscopy. IR spectra were obtained at room temperature using a Mattson Galaxy 4030 series FT-IR spectrophotometer. IR samples were prepared in a drybox by dissolving 5−10 mg of $(^{5/6}L)Fe^{II}$, $[(^{5/6}L)Fe^{II}\cdots Cu^{I}](B(C_6F_5)_4)$, or $[(TMPA)Cu^{I}(CH_3CN)](B(C_6F_5)_4)$ in ~1 mL solvent in a vial. In samples in which the exogenous axial ligand base 1,5-dicyclohexylimidazole

(39) Collman, J. P.; Sunderland, C. J.; Boulatov, R. *Inorg. Chem.* **2002**, *41*, 2282−2291.
(40) Ghiladi, R. A.; Lee, D.-H.; Huang, H.-w.; Moënne-Loccoz, P.; Kaderli, S.; Zuberbühler, A. D.; Woods, A. S.; Cotter, R. J.; Karlin, K. D. Manuscript in preparation.
(41) Liang, H.-C.; Kim, E.; Incarvito, C. D.; Rheingold, A. L.; Karlin, K. D. *Inorg. Chem.* **2002**, *41*, 2209−2212.
(42) Karlin, K. D.; Hayes, J. C.; Shi, J.; Hutchinson, J. P.; Zubieta, J. *Inorg. Chem.* **1982**, *21*, 4106−4108.
(43) Karlin, K. D.; Cruse, R. W.; Gultneh, Y.; Farooq, A.; Hayes, J. C.; Zubieta, J. *J. Am. Chem. Soc.* **1987**, *109*, 2668−2679.
(44) Karlin, K. D.; Haka, M. S.; Cruse, R. W.; Meyer, G. J.; Farooq, A.; Gultneh, Y.; Hayes, J. C.; Zubieta, J. *J. Am. Chem. Soc.* **1988**, *110*, 1196−1207.

Table 1. UV−Vis Data (nm) for Fe/Empty-Tether Compounds at Room Temperature

solvent	$(^5L)Fe^{II}$ [a]	$(^5L)Fe^{II}-CO$ [a]	$(^6L)Fe^{II}$ [b]	$(^6L)Fe^{II}-CO$ [b]
THF (Soret)	424	414	424	413
	$(2.32 \pm 0.14) \times 10^5$	$(3.2 \pm 0.2) \times 10^5$	$(2.40 \pm 0.014) \times 10^5$	$(3.16 \pm 0.16) \times 10^5$
α	544	533	543	532
	$(1.18 \pm 0.03) \times 10^4$	$(1.50 \pm 0.06) \times 10^4$	$(1.0 \pm 0.2) \times 10^4$	$(1.4 \pm 0.08) \times 10^4$
acetonitrile (Soret)	424	415	426	415
α	530, 555(sh)	540	530, 555(sh)	539
acetone (Soret)	429	414	429	413
α	535(sh), 557	534	536(sh), 556	534
toluene (Soret)	416, 431	416	417(sh), 433	419
α	532, 558(sh)	535	534, 556(sh)	537
CH_2Cl_2 (Soret)	416(sh), 431	416	416(sh), 434	419
α	536(sh), 557	536	538(sh), 557	538

[a] Extinction coefficients were determined based on three trials. [b] Extinction coefficients were determined based on two trials.

(DCHIm) was added, 1 equiv was weighed out in the drybox and added to the solution prior to carbonylation. The vial was then sealed with a 14/20 rubber septum prior to removal to the benchtop. After taking an IR spectrum using a SPECAC solution cell of the $(^{5/6}L)Fe^{II}$, $[(^{5/6}L)Fe^{II}\cdots Cu^{I}](B(C_6F_5)_4)$, or $[(TMPA)Cu^{I}(CH_3CN)](B(C_6F_5)_4)$ sample as a control, the stock solution in the vial was bubbled with CO for 5−10 s. An IR spectrum was then taken of the carbonylated species in order to observe the specific $(CO)_{Fe}$ and/or $(CO)_{Cu}$ stretching frequency.

In an attempt to generate the $[(^{5/6}L)Fe^{II}-CO\cdots Cu^{I}](B(C_6F_5)_4)$ species, the $[(^{5/6}L)Fe^{II}\cdots Cu^{I}](B(C_6F_5)_4)$ stock solution was first bubbled with CO and then followed by Ar bubbling for 5−10 s. After transfer to the solution cell, an IR spectrum was taken as previously described.

A complex formulated as $[(PY1)Cu^{I}-CO](B(C_6F_5)_4)$ {PY1 = bis(2-picolyl)amine (Richmond Chemicals)} was generated in situ by dissolving 22 mg PY1 and 100 mg $[Cu^{I}(CH_3CN)_4](B(C_6F_5)_4)$ in ∼5 mL CH_3CN, followed after 45 min of stirring by the addition of CO.

^{1}H and ^{2}H NMR Spectroscopy. ^{1}H and ^{2}H NMR spectra were recorded at room temperature on a Varian Unity 400 NMR spectrometer (^{1}H at 400 MHz, ^{2}H at 61.3 MHz). ^{1}H NMR samples were prepared in a glovebox by dissolving 20−30 mg of $(^{5/6}L)Fe^{II}$, $[(^{5/6}L)Fe^{II}\cdots Cu^{I}](B(C_6F_5)_4)$, $(F_8TPP)Fe^{II}$, or $[(TMPA)Cu^{I}(CH_3CN)](B(C_6F_5)_4)$ in 1 mL of deuterated NMR solvent in a 5 mm, airtight, screw-cap NMR tube (Wilmad Glass). After a spectrum of the reduced sample was obtained, carbonylation was effected by bubbling CO through the sample via syringe needle for 5−10 s.

^{2}H NMR spectra were collected using a tunable broadband probe to enhance ^{2}H detection. Samples were prepared by dissolving 20−30 mg of $(^5L\text{-}d_8)Fe^{II}$ in 1 mL of solvent (undeuterated) in a screw-cap NMR tube, followed by carbonylation as already described. ^{2}H NMR spectra of $[(^5L\text{-}d_8)Fe^{II}\cdots Cu^{I}](B(C_6F_5)_4)$ were prepared in situ as previously described. Chemical shifts are reported as δ values internally referenced to solvent.

^{13}C NMR Spectroscopy. ^{13}C NMR spectra were also collected on a Varian Unity 400 NMR spectrometer at 100 MHz using a tunable broadband probe to enhance ^{13}C detection. Samples of $(^{5/6}L)Fe^{II}$, $[(^5L)Fe^{II}\cdots Cu^{I}](B(C_6F_5)_4)$, $(F_8TPP)Fe^{II}$, and $[(TMPA)Cu^{I}(CH_3CN)](B(C_6F_5)_4)$ were prepared in an analogous fashion to those already described for the ^{1}H NMR spectroscopic studies. However, carbonylation was effected by using a 3-way T-valve syringe assembly to bubble each sample with 2 × 5 mL isotopically labeled ^{13}CO stored in 100 mL breakseals (ICON Services, Inc.). For $(^{5/6}L)Fe^{II}-CO$ and $(F_8TPP)Fe^{II}-CO$, spectra were taken in THF-d_8 and CD_2Cl_2 using ^{13}CO 67% enriched in ^{13}C, while spectra for the $[(^{5/6}L)Fe^{II}-CO\cdots Cu^{I}-CO](B(C_6F_5)_4)$ and $[(TMPA)Cu^{I}-CO](B(C_6F_5)_4)$ samples were taken in THF-d_8 using 99% enriched ^{13}CO. Chemical shifts are reported as δ values internally referenced to solvent peaks.

Results and Discussion

Synthesis and Characterization. The Fe/empty-tether species, $(^{5/6}L)Fe^{II}$ and $(^6L\text{-}d_8)Fe^{II}$ (Chart 1), and the Fe/Cu complexes $[(^{5/6}L)Fe^{II}\cdots Cu^{I}](BArF_{20})$ and $[(^6L\text{-}d_8)Fe^{II}\cdots Cu^{I}](B(C_6F_5)_4)$, have been synthesized and characterized as described in the preceding section, or elsewhere.[25,40] The deuterated compounds $(^5L\text{-}d_8)Fe^{II}$ and $[(^5L\text{-}d_8)Fe^{II}\cdots Cu^{I}](B(C_6F_5)_4)$ were synthesized in an analogous fashion to that reported for the deuterated ^{6}L ligand.[40]

Five organic solvents were chosen for study of the Fe/empty-tether species with carbon monoxide. These were acetonitrile, tetrahydrofuran, acetone, toluene, and methylene chloride, ranging from strongly coordinating to noncoordinating, in their ability to interact with iron(II).[20] These solvents have been shown to have a marked effect on the iron(II) spin-state and have also yielded variations in dioxygen reactivity, in the electronically similar $(F_8TPP)Fe^{II}$ system.[20,45] For this reason, their effect on carbonyl chemistry is also of interest. For the Fe/Cu species, all but methylene chloride were used due to its reaction with $Cu^{I}(TMPA)$ species, yielding $Cu^{II}-Cl$.[46]

UV−Vis Spectroscopy. In general, addition of CO caused an immediate color change in the dilute samples (Soret band, with absorption ∼0.5−1.0) from yellow to light tan. In the more concentrated (∼10×) samples used to measure absorption bands in the α region, the color changed from a deep orange/brown to red. Overall, for both the Fe/empty-tether and Fe/Cu species, carbonylation of the sample resulted in a blue shift for both the Soret and α bands and loss of any double-featured characteristics in the Soret or α region. Addition of CO was marked by a sharpening of the Soret feature in each case and an increase in intensity in both the Soret and α absorptions, as determined by measurements of the extinction coefficients (ϵ) in THF for $(^{5/6}L)Fe^{II}$ and $(^{5/6}L)Fe^{II}-CO$ (Table 1). Such changes upon carbonylation have been observed in related porphyrin systems.[47] In fact, there is almost no variation in λ_{max} values from solvent to

(45) Ghiladi, R. A.; Karlin, K. D. *Inorg. Chem.* **2002**, *41*, 2400−2407.
(46) Jacobson, R. R.; Tyeklár, Z.; Karlin, K. D. *Inorg. Chim. Acta* **1991**, *181*, 111−118.
(47) Traylor, T. G.; Chang, C. K.; Geibel, J.; Berzinis, A.; Mincey, T.; Cannon, J. *J. Am. Chem. Soc.* **1979**, *101*, 6716−6730.

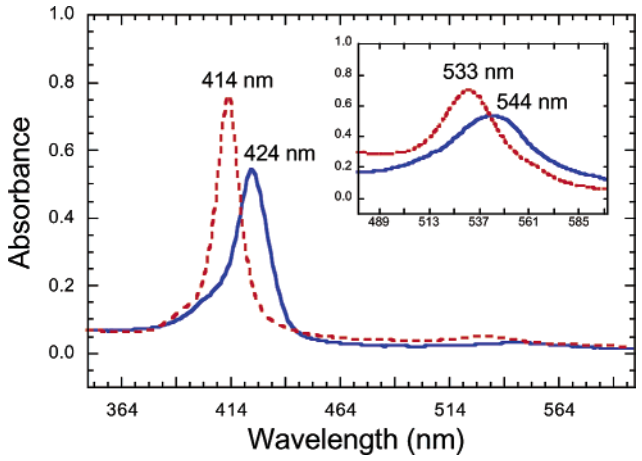

Figure 2. Overlayed UV−vis spectra of (^{5}L)Fe^{II} (−−) and (^{5}L)Fe^{II}−CO (- -) in THF at room temperature. A more concentrated spectrum of the α region for each sample is included.

solvent (Table 1), and use of either constitutional isomer (^{5}L vs ^{6}L) did not significantly alter the observed optical spectra.

($^{5/6}$L)Fe^{II} Carbonylation. UV−vis spectra of ($^{5/6}$L)Fe^{II} before carbonylation revealed a marked effect of solvent on both peak shape and position (Table 1). It is useful to note that in weakly coordinating solvents, e.g., CH_2Cl_2, toluene, and possibly acetone, a pyridine arm from the tether may coordinate to the heme (see diagram).[45]

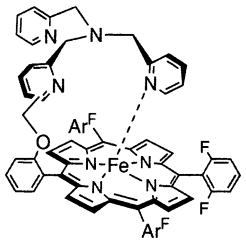

($^{5/6}$L)Fe^{II}

Here we highlight the UV−vis changes for (^{5}L)Fe^{II} in THF {UV−vis: 424 (Soret), 544 nm}. After carbonylation, the (^{5}L)Fe^{II}−CO spectral features shifted to 414 (Soret) and 533 nm (Figure 2); similar spectral changes are observed for the formation of (^{6}L)Fe^{II}−CO (Table 1). The results show clear UV−vis changes that are analogous to those of other heme complexes and proteins.[48,49] We conclude this addition of CO causes the species to become six-coordinate, low-spin (see also NMR spectroscopic evidence, vide infra), with either a solvent molecule or a pyridine arm occupying the sixth coordination site on the iron(II) (Chart 2, where B = solvent axial base). The CO molecule may be on the "tether side" of the porphryin plane or bound to the open face, as also suggested for O_2-coordination.[45]

[($^{5/6}$L)Fe^{II}···Cu^{I}](B(C$_6$F$_5$)$_4$) Carbonylation. UV−vis spectra for the [($^{5/6}$L)Fe^{II}···Cu^{I}](B(C$_6$F$_5$)$_4$) and [($^{5/6}$L)Fe^{II}−CO··Cu^{I}−CO](B(C$_6$F$_5$)$_4$) samples yielded similar features to their ($^{5/6}$L)Fe^{II} and ($^{5/6}$L)Fe^{II}−CO counterparts; thus, the presence of copper(I) in the ^{5}L or ^{6}L tether seemed to have little or no effect on electronic absorption spectra in the solvents tested, since the heme dominates in UV−vis spectra and copper(I) complexes (d^{10}) generally do not show charge-transfer or d−d absorptions in the visible region. Two examples in support of this conclusion follow: In toluene, [(^{5}L)Fe^{II}···Cu^{I}](B(C$_6$F$_5$)$_4$) exhibited multiple Soret and α bands as in the Fe/empty tether system,[45] with absorptions at 413, 432(sh) (Soret), and 530, 556(sh) nm. Upon carbonylation, the peak positions changed to 418 (Soret) and 535 nm. Similarly, [(^{6}L)Fe^{II}···Cu^{I}](B(C$_6$F$_5$)$_4$) in toluene produced 415, 435(sh) (Soret), and 530, 556(sh) nm absorptions, followed by 417 (Soret) and 533 nm peaks after addition of CO. In THF, [(^{6}L)Fe^{II}···Cu^{I}](B(C$_6$F$_5$)$_4$) showed single-featured Soret and α bands at 424 and 546 nm, as in ($^{5/6}$L)Fe^{II}.[45] Upon carbonylation, these bands shifted to 413 (Soret) and 532 nm, identical to the absorptions in (^{6}L)Fe^{II}−CO.

Chart 2

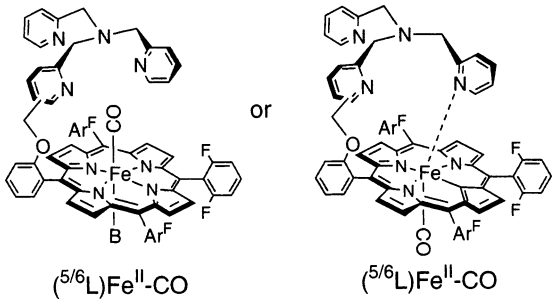

Table 2. ν(CO)$_{Fe}$ (cm^{-1}) IR Data at Room Temperature

solvent	(^{5}L)Fe^{II}−CO	(^{6}L)Fe^{II}−CO	[(^{5}L)Fe^{II}−CO···Cu^{I}−CO]-(B(C$_6$F$_5$)$_4$)	[(^{6}L)Fe^{II}−CO···Cu^{I}−CO]-(B(C$_6$F$_5$)$_4$)
THF	1978	1976	1973	1971
acetonitrile	1980	1978	1979	1977
acetone	1968	1969	1968	1968
toluene	1975	1975	1973	1970
CH_2Cl_2	1969	1976		

IR Spectroscopy. The same solvents used for the UV−vis spectroscopic studies were employed in order to determine their relative ability to act as an axial base ligand for the iron in the presumed (solvent)Fe^{II}−CO six-coordinate complex. As is well-known for binding of transition metals to carbon monoxide, and predicted for the present Fe−CO and/or Fe−CO/Cu−CO systems, both ν(CO)$_{Fe}$ and ν(CO)$_{Cu}$ values were found at lower energy than the 2143 cm^{-1} expected from free CO (vide infra). Table 2 provides ν(CO)$_{Fe}$ IR data for ($^{5/6}$L)Fe^{II}−CO and [($^{5/6}$L)Fe^{II}−CO···Cu^{I}−CO]-(B(C$_6$F$_5$)$_4$) in various solvents.

($^{5/6}$L)Fe^{II} Carbonylation and Effect of Added Base. In general, ν(CO)$_{Fe}$ values for ($^{5/6}$L)Fe^{II}−CO were found from 1968 to 1980 cm^{-1}, showing a modest dependence on the solvent used; an infrared spectrum of a typical carbonylation reaction is given in Figure 3 for (^{5}L)Fe^{II}. These stretching frequencies agree favorably with those observed for the "parent" reference compound (F$_8$TPP)Fe^{II}−CO, with ν(CO)$_{Fe}$

(48) Tsuchida, E.; Komatsu, T.; Arai, K.; Nishide, H. *J. Chem. Soc., Dalton Trans.* **1993**, 2465−2469.
(49) Collman, J. P.; Brauman, J. I.; Doxsee, K. M.; Halbert, T. R.; Bunnenberg, E.; Linder, R. E.; La Mar, G. N.; Del Gaudio, J.; Lang, G.; Spartalian, K. *J. Am. Chem. Soc.* **1980**, *102*, 4182−4192.

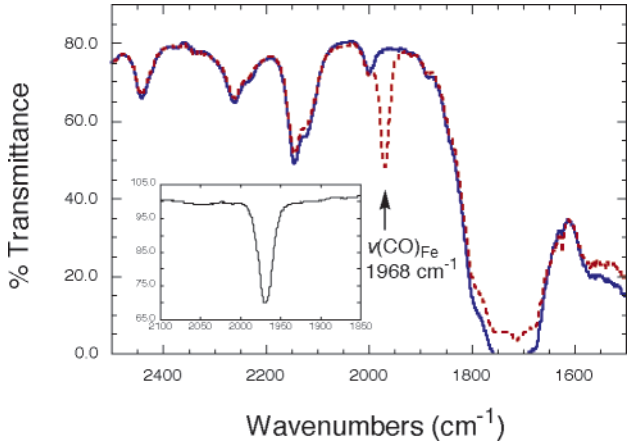

Figure 3. Overlayed IR spectra of (^{5}L)Fe^{II} (——) and (^{5}L)Fe^{II}-CO (- -) in acetone at room temperature. A difference spectrum appears as an inset.

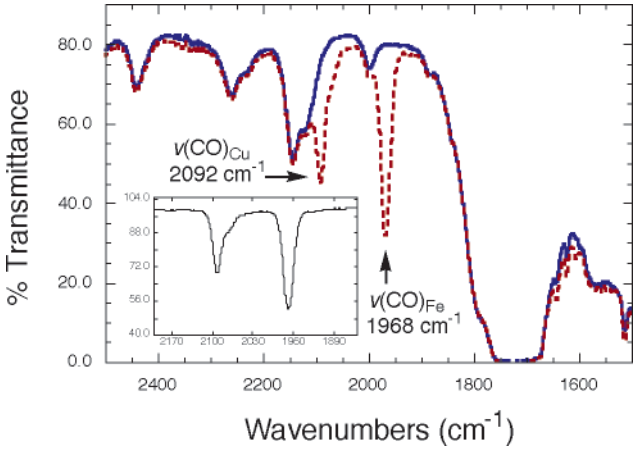

Figure 4. Overlayed IR spectra of [(^{5}L)Fe^{II}···Cu^I](B(C$_6$F$_5$)$_4$) (——) and [(^{5}L)Fe^{II}−CO···Cu^I−CO](B(C$_6$F$_5$)$_4$) (- -) in acetone at room temperature. A difference spectrum appears as an inset.

values of 1976 cm^{-1} (acetone), 1979 cm^{-1} (THF), and 1982 cm^{-1} (acetonitrile).[50] For other related porphyrin macrocycles, including "capped" and "pocket" porphyrins, similar ν(CO)$_{Fe}$ values are observed.[48,51−53] Note the similar values for the hemoproteins myoglobin (ν(CO)$_{Fe}$ = 1945 cm^{-1}) and hemoglobin (ν(CO)$_{Fe}$ = 1951 cm^{-1}).[52]

In order to determine the effect of a nonsolvent derived strongly donating axial base ligand, 1 equiv of 1,5-dicyclohexylimidazole was added to a sample of (^{5}L)Fe^{II} in toluene prior to carbonylation. A ν(CO)$_{Fe}$ absorption at 1984 cm^{-1} was observed, representing a shift of 9 cm^{-1} from the 1975 cm^{-1} stretch found for (^{5}L)Fe^{II}−CO in toluene. Note that among the coordinating solvents (THF, MeCN, and acetone), both THF and MeCN provide ($^{5/6}$L)Fe^{II}−CO complexes with the greatest ν(CO)$_{Fe}$ stretching frequencies (Table 2), consistent with our previously[20,45] derived notions of their relative strength of coordination to the heme (i.e., THF > MeCN > acetone).

[($^{5/6}$L)Fe^{II}···Cu^I](B(C$_6$F$_5$)$_4$) Carbonylation. For the [($^{5/6}$L)-Fe^{II}-CO···Cu^I−CO](B(C$_6$F$_5$)$_4$) species, ν(CO)$_{Fe}$ values analogous to those in empty-tether ($^{5/6}$L)Fe^{II}−CO species were observed, ranging from 1968 to 1979 cm^{-1} (Table 2 and Figure 4).

IR spectra of the Cu^I−CO moiety in [($^{5/6}$L)Fe^{II}−CO··· Cu^I−CO](B(C$_6$F$_5$)$_4$) complexes, obtained by directly bubbling carbon monoxide through solutions of the reduced samples under an inert atmosphere, exhibited a strong absorption in the range 2091−2094 cm^{-1} (Table 3 and Figure 4). These values are typical for copper complexes although somewhat higher in energy than for Cu−CO moieties in metalloproteins.[54,55]

Table 3. ν(CO)$_{Cu}$ (cm^{-1}) IR Data at Room Temperature

solvent	[(^{5}L)Fe^{II}−CO··· Cu^I−CO]-(B(C$_6$F$_5$)$_4$)	[(^{6}L)Fe^{II}−CO···Cu^I−CO]-(B(C$_6$F$_5$)$_4$)	[(TMPA)-Cu^I−CO]-(B(C$_6$F$_5$)$_4$)	[(PY1)Cu^I−CO]-(B(C$_6$F$_5$)$_4$)
THF	2091	2093	2091	
acetonitrile	2094	2092	2092	2091
acetone	2092	2093	2092	
toluene	2093	2093	2091	

Chart 3

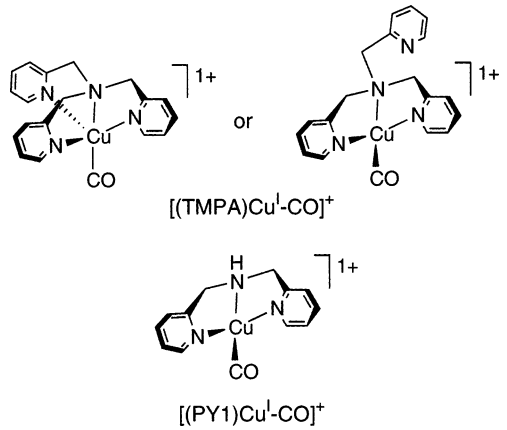

The Cu^I−CO infrared region for [($^{5/6}$L)Fe^{II}−CO···Cu^I−CO](B(C$_6$F$_5$)$_4$) also exhibited a weaker shoulder at lower energy, ∼2070 cm^{-1} (see Figure 4 inset), which varied in intensity with the solvent used. However, in toluene the shoulder was more pronounced, appearing as a separate peak at 2068 cm^{-1} in [(^{5}L)Fe^{II}−CO···Cu^I−CO](B(C$_6$F$_5$)$_4$) and at 2037 cm^{-1} in [(^{6}L)Fe^{II}−CO···Cu^I−CO](B(C$_6$F$_5$)$_4$). In order to gain insight into the origin of the ν(CO)$_{Cu}$ absorptions, including this weak but persistent shoulder, control experiments were performed utilizing [(TMPA)Cu^I(CH$_3$CN)]-(B(C$_6$F$_5$)$_4$) and [(PY1)Cu^I(CH$_3$CN)](B(C$_6$F$_5$)$_4$) (Chart 3).

Upon addition of CO to each compound in solution, a color change was seen from yellow to colorless. IR experiments using [(TMPA)Cu^I−CO](B(C$_6$F$_5$)$_4$) yielded spectra with ν(CO)$_{Cu}$ values from 2091 to 2092 cm^{-1}, but also exhibiting a shoulder in the 2068−2071 cm^{-1} range that varied in intensity with solvent. Thus, the Cu moiety in the [($^{5/6}$L)Fe^{II}···Cu^I]$^+$ complexes binds CO in a manner that appears to be independent of the heme.

(50) Thompson, D. W.; Kretzer, R. M.; Lebeau, E. L.; Scaltrio, D.; Ghiladi, R. A.; Lam, K.-C.; Rheingold, A. L.; Meyer, G. J.; Karlin, K. D. Manuscript in preparation.
(51) Linard, J. E.; Ellis, P. E., Jr.; Budge, J. R.; Jones, R. D.; Basolo, F. *J. Am. Chem. Soc.* **1980**, *102*, 1896−1904.
(52) Collman, J. P.; Brauman, J. I.; Collins, T. J.; Iverson, B. L.; Lang, G.; Pettman, R. B.; Sessler, J. L.; Walters, M. A. *J. Am. Chem. Soc.* **1983**, *105*, 3038−3052.
(53) Collman, J. P.; Reed, C. A. *J. Am. Chem. Soc.* **1973**, *95*, 2048−2049.
(54) Rondelez, Y.; Séneque, O.; Rager, M.-N.; Duprat, A. F.; Reinaud, O. *Chem. Eur. J.* **2000**, *6*, 4218−4226.
(55) Hirota, S.; Iwamoto, T.; Tanizawa, K.; Aduchi, O.; Yamauchi, O. *Biochemistry* **1999**, *38*, 14256−14263.

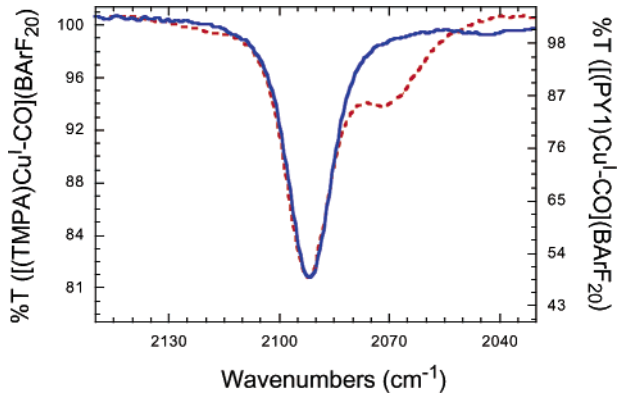

Figure 5. Overlayed IR difference spectra of $[(PY1)Cu^{I}-CO](B(C_6F_5)_4) - [(PY1)Cu^{I}(CH_3CN)](B(C_6F_5)_4)$ (——) and $[(TMPA)Cu^{I}-CO](B(C_6F_5)_4) - [(TMPA)Cu^{I}(CH_3CN)](B(C_6F_5)_4)$ (- -) in CH_3CN at room temperature. The spectra have been normalized to account for differences in absorbance due to variations in concentrations.

An experiment with $[(PY1)Cu^{I}(CH_3CN)](B(C_6F_5)_4)$ (Chart 3) bubbled with CO in CH_3CN gave more insight into the likely origin of the IR shoulder. $[(PY1)Cu^{I}(CH_3CN)](B(C_6F_5)_4)$ differs from $[(TMPA)Cu^{I}(CH_3CN)](B(C_6F_5)_4)$ in that only two pyridine moieties are present to bind Cu, as opposed to three in TMPA. Upon addition of CO to the $[(PY1)Cu^{I}(CH_3CN)](B(C_6F_5)_4)$ species in CH_3CN (see Experimental Section), an IR stretch was observed at 2091 cm^{-1}, identical to the major peak seen at 2092 cm^{-1} for $[(TMPA)Cu^{I}-CO](B(C_6F_5)_4)$ in CH_3CN. A difference spectrum was generated in which the IR spectrum of $[(PY1)Cu^{I}(CH_3CN)](B(C_6F_5)_4)$ was subtracted from that of $[(PY1)Cu^{I}-CO](B(C_6F_5)_4)$, showing only the 2091 cm^{-1} stretch with no shoulder at ~2070 cm^{-1} (Figure 5).

These observations provide good evidence that the predominate species in solutions contains a single uncoordinated pyridyl arm of the TMPA ligand, both for $[(TMPA)Cu^{I}-CO](B(C_6F_5)_4)$ and $[(^{5/6}L)Fe^{II}-CO\cdots Cu^{I}-CO](B(C_6F_5)_4)$. We therefore propose that the shoulder at ~2070 cm^{-1} could then correspond to a species in which all three pyridyl arms of the TMPA moiety are coordinated to the copper(I) ion complex (Chart 3). This hypothesis seems logical as the coordination of three pyridyl arms to the copper(I) would increase the electron density around this metal, thereby decreasing the strength, and in turn the stretching frequency, of the C−O bond. This assumption seems to be further supported by the presence of an even more prominent peak at ~2070 cm^{-1} in toluene upon CO addition, as toluene is a noncoordinating solvent, making it more likely that all three pyridyl donors coordinate in the CO-adduct. Furthermore, previous experiments in which PPh_3 was added to $[(TMPA)Cu^{I}](PF_6)$ have shown that a pyridyl arm can "dangle", leaving tridentate coordination from the potentially tetradentate TMPA chelated.[56]

Possible Solution-State Structures of $[(^{5/6}L)Fe^{II}-CO\cdots Cu^{I}-CO](B(C_6F_5)_4)$. On the basis of the IR experiments comparing the CO binding of $[(PY1)Cu^{I}-CO](B(C_6F_5)_4)$ and $[(TMPA)Cu^{I}-CO](B(C_6F_5)_4)$, four isomeric

Scheme 1

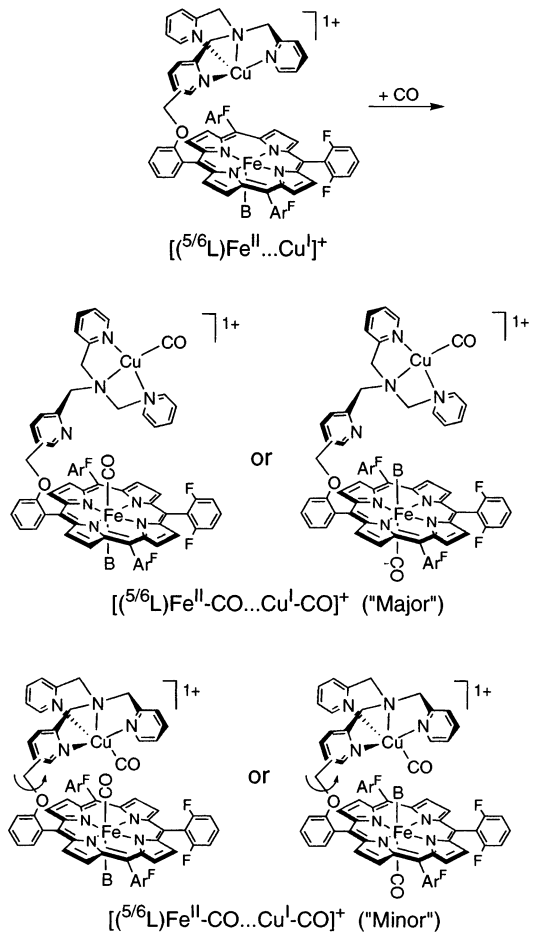

carbonyl species are possible for the $[(^{5/6}L)Fe^{II}-CO\cdots Cu^{I}-CO](B(C_6F_5)_4)$ complexes (Scheme 1). With respect to $Cu^{I}-CO$ adduct formation, the relative intensities of the two $(CO)_{Cu}$ IR stretches point to the "major" product of the carbonylation reaction containing a "dangling" pyridine arm which is not coordinated to the copper(I). By analogy to the geometry of $[(PY1)Cu^{I}-CO](B(C_6F_5)_4)$, this accounts for the IR stretch at 2091−2094 cm^{-1} (Table 3). The noncoordinated pyridyl moiety is assumed to be that which is directly tethered to the heme via an ether linkage, as the previously described crystal structure of $[(^{6}L)Fe^{III}-O-Cu^{II}](B(C_6F_5)_4)$ showed this Cu−N bond to be elongated by ~0.4 Å relative to the other two.[25] This allows the tethered $(TMPA)Cu^{I}$ to rotate away from the porphyrin ring plane. For this $(TMPA)Cu^{I}$ conformation, two possible isomers exist for CO binding to the ferrous heme, one in which the CO is on the same side as the tethered $(TMPA)Cu^{I}$, and one in which it is on the opposite side. In order to account for the $(CO)_{Cu}$ IR stretch at ~2070 cm^{-1}, it is likely that the "minor" product (Scheme 1) involves weak coordination of the third pyridyl arm to the copper(I), which could potentially localize the $(TMPA)Cu^{I}$ over the heme to form a sterically hindered binding pocket. However, due to free rotation about the either linkage of the tether, it is also possible that the $TMPA(Cu^{I})$ rotates from 0° to 180° relative to the porphyrin. This conformation in which the copper(I) has three coordinated pyridyl arms also has two possible isomers for heme-CO

(56) Tyeklár, Z.; Jacobson, R. R.; Wei, N.; Murthy, N. N.; Zubieta, J.; Karlin, K. D. *J. Am. Chem. Soc.* **1993**, *115*, 2677−2689.

Scheme 2

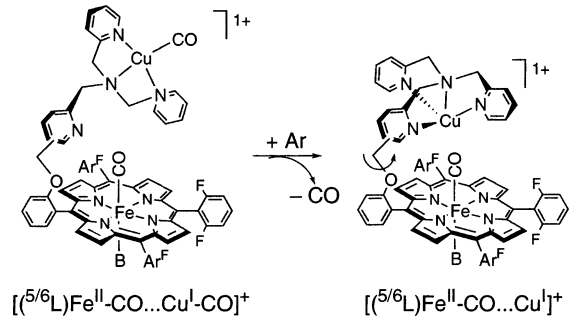

binding, as shown. In all possible geometric isomers, the sixth ligand-coordination site can be occupied by a solvent molecule such as THF (B = axial ligand base, Scheme 1).

Further evidence for these formulations comes from the observed invariability of the $\nu(CO)_{Fe}$ in both the Fe/empty-tether and the Fe/Cu systems. If the (TMPA)Cu^I moiety was primarily localized in close proximity to the heme, forming an Fe/Cu binding pocket, then one might expect a decrease in $\nu(CO)_{Fe}$ in the [($^{5/6}$L)Fe^{II}−CO···Cu^I−CO](B(C_6F_5)$_4$) species relative to ($^{5/6}$L)Fe^{II}−CO due to interaction of the positively charged copper(I) with $(CO)_{Fe}$. Collman and coworkers[39] have elaborated on this phenomenon, noting that (i) such an interaction would serve to stabilize the Fe-d_π-to-CO-π^* back-bonding interaction, thereby weakening the CO bond, (ii) citing biological precendence, where in mutants of cytochrome *bo* ubiquinol oxidase (from *E. coli*), and other terminal oxidases in which the ability to bind copper(I) was removed, there is an increase in $\nu(CO)_{Fe}$ relative to the wild type,[57−59] and (iii) in general, Fe−C−O prefers a linear geometry in order to maximize the back-bonding stabilization, and steric effects that alter this geometry from linearity have been associated with changes in $\nu(CO)_{Fe}$ values.[3,60−65] However, no significant difference in $\nu(CO)_{Fe}$ was observed in comparing [($^{5/6}$L)Fe^{II}−CO···Cu^I−CO](B(C_6F_5)$_4$) and ($^{5/6}$L)-Fe^{II}−CO species; thus, it is likely that the copper(I) ion in these Fe/Cu systems is not close enough to significantly interact with the Fe−CO unit.

Selective Binding to Fe; Generation of Base−Fe^{II}−CO···Cu^I. Using the same stock solution of [($^{5/6}$L)Fe^{II}···Cu^I]-(B(C_6F_5)$_4$) that was used to generate the bis-carbonyl (i.e., Fe−CO/Cu−CO) species, samples first bubbled with CO were now followed by Ar for 5−10 s, in an effort to selectively displace the CO bound to the copper(I) and generate the [($^{5/6}$L)Fe^{II}−CO···Cu^I](B(C_6F_5)$_4$) species (Scheme 2).

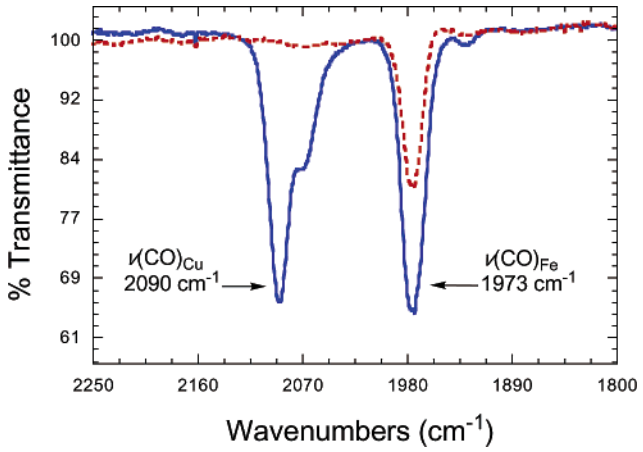

Figure 6. Overlayed IR difference spectra of ([(^{5}L)Fe^{II}−CO···Cu^I−CO]$^+$ + DCHIm) − ([(^{5}L)Fe^{II}···Cu^I]$^+$ + DCHIm) (−−) and ([(^{5}L)Fe^{II}−CO···Cu^I]$^+$ + DCHIm) − ([(^{5}L)Fe^{II}···Cu^I]$^+$ + DCHIm) (- -) in THF at room temperature. DCHIm (1 equiv) was added to the solution prior to CO bubbling, and the [(^{5}L)Fe^{II}−CO···Cu^I]$^+$ species was generated by bubbling with Ar.

Table 4. ^{1}H NMR Data (δ, ppm) for Fe/Empty-Tether Compounds at Room Temperature

solvent	(^{5}L)Fe^{II}	(^{5}L)Fe^{II}−CO	(^{6}L)Fe^{II}	(^{6}L)Fe^{II}−CO
THF-d_8	55.4, 55.7, 56.9, 57.5	8.8	52.9, 54.2, 57.8. 58.6	8.8
acetonitrile-d_3	30.0, 30.9, 31.2, 31.6	8.8	41.1, 42.8, 43.6, 44.5	8.8
acetone-d_6	47.3, 48.6, 49.8, 50.4	8.8	48.2, 50.1, 51.8, 52.5	8.8
toluene-d_8	31−37 (v br)	8.7	31.8, 32.8, 34.5	8.8
CD_2Cl_2	43.6 (br)	8.7	44.2, 45.7, 47.3, 48.1	8.9

This resulted in the nearly complete loss of CO from the Cu(I), as proven by a disappearance of the stretch at ∼2090 cm^{-1} in IR spectra. Loss of intensity of the 1970 cm^{-1} $\nu(CO)_{Fe}$ band also occurred, but the extent was solvent dependent, following the general trend acetone (∼60% loss) > MeCN (∼35% loss) > THF > THF with added 1,5-dicyclohexylimidazole (DCHIm, 1 equiv; ∼40% loss, Figure 6). Thus, these experiments are consistent with solvent or axial base ligand (DCHIm) binding to the heme and stabilizing the Fe−CO interaction. We previously observed a very similar solvent coordination trend for just the heme−Fe(II).[20,45]

^{1}H and ^{2}H NMR Spectroscopy. ($^{5/6}$L)Fe^{II}, (^{5}L-d_8)Fe^{II}, and CO-Adducts. ^{1}H NMR spectra of reduced ($^{5/6}$L)Fe^{II} prior to carbonylation yielded from one to four distinct pyrrole resonances in the (δ) 25−60 ppm range depending on the solvent used, as previously published.[20,45] Coordinating solvents, such as THF-d_8, acetonitrile-d_3, and acetone-d_6, yielded four well-defined pyrrole peaks for both the ($^{5/6}$L)Fe^{II} species (Table 4). However, for (^{5}L)Fe^{II} in toluene-d_8 and dichloromethane-d_2, the downfield shifted pyrrole signature was broad and poorly defined. This was not the case for the (^{6}L)Fe^{II} compound. For acetonitrile-d_3, the pyrrole resonance positions are indicative of a thermal equilibrium between five-coordinate (mono-MeCN) high-spin and six-coordinate

(57) Calhoun, M. W.; Hill, J. J.; Lemieux, L. J.; Ingledew, W. J.; Alben, J. O.; Gennis, R. B. *Biochemistry* **1993**, *32*, 11524−11529.
(58) Uno, T.; Mogi, T.; Tsubaki, M.; Nishimura, Y.; Anraku, Y. *J. Biol. Chem.* **1994**, *269*, 11912−11920.
(59) Hosler, J. P.; Kim, Y.; Shapleigh, J.; Gennis, R. B.; Alben, J. O.; Ferguson-Miller, S.; Babcock, G. T. *J. Am. Chem. Soc.* **1994**, *116*, 5515−5516.
(60) Park, K. D.; Guo, K.; Adebodun, F.; Chiu, M. L.; Sligar, S. G.; Oldfield, E. *Biochemistry* **1991**, *30*,
(61) Ray, G. B.; Li, X.-Y.; Ibers, J. A.; Sessler, J. L.; Spiro, T. G. *J. Am. Chem. Soc.* **1994**, *116*, 162−176.
(62) Tetreau, C.; Lavalette, D.; Momenteau, M.; Fischer, J.; Weiss, R. *J. Am. Chem. Soc.* **1994**, *116*, 11840−11848.
(63) Slebodnick, C.; Duval, M. L.; Ibers, J. A. *Inorg. Chem.* **1996**, *35*, 3607−3613.
(64) Vogel, K. M.; Kozlowski, P. M.; Zgierski, M. Z.; Spiro, T. G. *Inorg. Chim. Acta* **2000**, *297*, 11−17.
(65) Kalodimos, C. G.; Gerothanassis, I. P.; Pierattelli, R.; Troganis, A. *J. Inorg. Biochem.* **2000**, *79*, 371−380.

Table 5. ^{1}H NMR Data (δ, ppm) for Fe/Cu Compounds at Room Temperature

solvent	[(^{5}L)Fe^{II}···Cu^I]-(B(C_6F_5)$_4$)	[(^{5}L)Fe^{II}−CO···Cu^I−CO]-(B(C_6F_5)$_4$)	[(^{6}L)Fe^{II}···Cu^I]-(B(C_6F_5)$_4$)	[(^{6}L)Fe^{II}−CO···Cu^I−CO]-(B(C_6F_5)$_4$)
THF-d_8	54.0, 54.7, 57.7, 58.8	8.74, 8.82	54.2, 56.7	8.75, 8.81, 8.86
acetonitrile-d_3	27.6 (sh), 28.7, 29.2	8.77	28.8 (sh), 29.8	8.74, 8.78, 8.81
acetone-d_6			45.9, 46.9, 48.2, 48.7	8.87

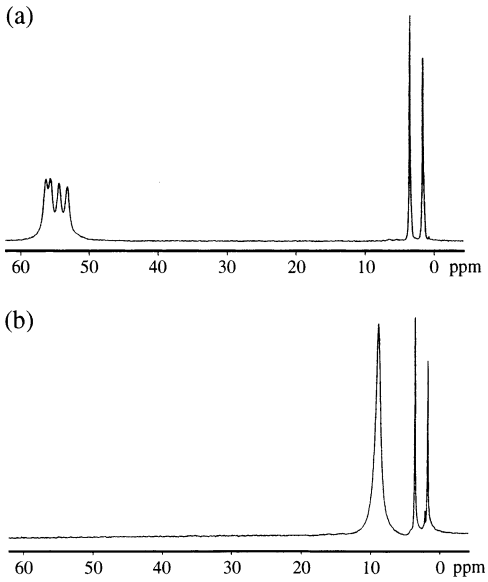

Figure 7. ^{2}H NMR spectra of (a) (^{5}L-d_8)Fe^{II} and (b) (^{5}L-d_8)Fe^{II}−CO in THF at room temperature. THF solvent peaks appear at 1.73 and 3.58 ppm in each spectrum.

(bis-MeCN) low-spin ferrous hemes, whereas in noncoordinating solvents (toluene-d_8, dichloromethane-d_2), a pyridyl group from the TMPA tether ligates the heme, vide supra.[20,45] Carbonylation in all cases yields an upfield shift in the pyrrole resonances to the diamagnetic region (8.7−8.9 ppm), analogous to what occurs for other five-coordinate, high-spin iron(II) heme compounds when CO or O_2 is added (Table 4).[66]

Further evidence in support of the pyrrole resonance assignments was aided by collection of ^{2}H NMR spectra obtained in THF for (^{5}L-d_8)Fe^{II} and (^{5}L-d_8)Fe^{II}−CO. This experiment yielded a group of four pyrrole peaks at 53.3, 54.5, 55.8, and 56.4 ppm for (^{5}L-d_8)Fe^{II}, and a single pyrrole resonance at 8.9 ppm for (^{5}L-d_8)Fe^{II}−CO (Figure 7).

[($^{5/6}$L)Fe^{II}···Cu^I](B(C_6F_5)$_4$), [(^{5}L-d_8)Fe^{II}···Cu^I](B(C_6F_5)$_4$), and CO-Adducts. ^{1}H NMR spectra for [($^{5/6}$L)Fe^{II}···Cu^I]-(B(C_6F_5)$_4$) were very similar to those found for the Fe/empty-tether compounds. However, in some cases it was possible to resolve more than one pyrrole peak after addition of CO in the 8.7−8.9 ppm range (Table 5).

^{2}H NMR spectra were also obtained in THF for [(^{5}L-d_8)-Fe^{II}···Cu^I](B(C_6F_5)$_4$) and [(^{5}L-d_8)Fe^{II}−CO···Cu^I−CO]-(B(C_6F_5)$_4$). For [(^{5}L-d_8)Fe^{II}···Cu^I](B(C_6F_5)$_4$), one broad pyrrole signature was found at 53.4 ppm, which shifted to 8.9 ppm upon addition of CO to yield [(^{5}L-d_8)Fe^{II}−CO···Cu^I−CO](B(C_6F_5)$_4$) (Figure 8). ^{2}H NMR of paramagnetic species, due to the quadrapolar relaxation of deuterons, often causes deuterium resonances to coalesce into a single, broad peak at the correct chemical shift but lacking the finer resolution found in ^{1}H NMR spectroscopy.[67,68] Thus, the results of the ^{1,2}H NMR spectroscopic studies indicate that the presence of the Cu^I−CO adduct in [($^{5/6}$L)Fe^{II}−CO···Cu^I−CO](B(C_6F_5)$_4$) complexes does not significantly affect the spin-state or coordination of the heme−Fe−CO species.

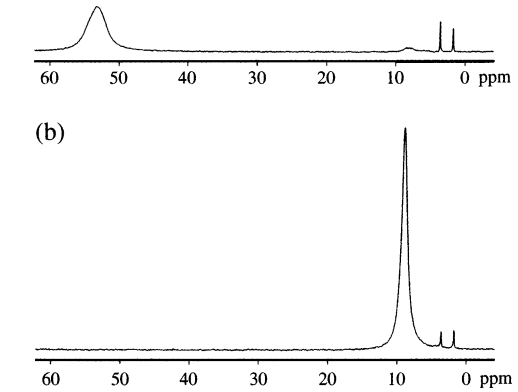

Figure 8. ^{2}H NMR spectra of (a) [(^{5}L-d_8)Fe^{II}···Cu^I](B(C_6F_5)$_4$) and (b) [(^{5}L-d_8)Fe^{II}−CO···Cu^I−CO](B(C_6F_5)$_4$) in THF at room temperature. THF solvent peaks appear at 1.73 and 3.59 ppm in each spectrum.

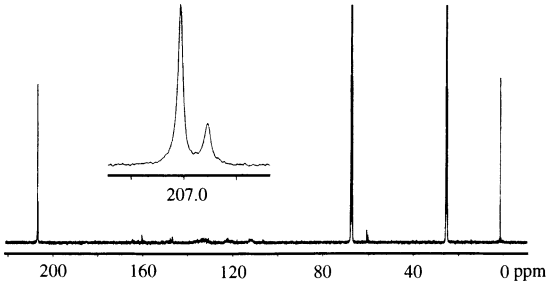

Figure 9. ^{13}C NMR spectra of (^{5}L)Fe^{II} + ^{13}CO (67% enriched in ^{13}C) in THF-d_8 at room temperature. The inset shows two resonance peaks at 206.8 and 207.0 ppm, both of which are assigned to (^{13}CO)$_{Fe}$. The two very intense upfield peaks (67 and 25 ppm) are due to the ^{13}C (at natural abundance) of the THF solvent, while the strong peak near 0 ppm is due to grease.

^{13}C NMR Spectroscopy of ^{13}CO-Adducts. In light of the interest in ^{13}C NMR spectroscopic data for (^{13}CO)-adducts of heme proteins and model complexes,[52,60,65,69] we wished to obtain corresponding data not only for our heme and heme-Cu compounds but also if possible for Cu^I−^{13}CO species. We are unaware of any ^{13}C NMR spectral data in the literature pertaining to a copper(I)-bound carbonyl group.

($^{5/6}$L)Fe^{II} Carbonylation. For the (^{5}L)Fe^{II}−CO sample in THF-d_8, two peaks were found that correspond to (^{13}CO)$_{Fe}$.

(66) Collman, J. P.; Fu, L. *Acc. Chem. Res.* **1999**, *32*, 455−463.

(67) Walker, F. A. In *The Porphyrin Handbook*; Kadish, K. M., Smith K. M., Guilard, R., Eds.; Academic Press: San Diego, CA, 2000; Vol. 5 (NMR and EPR), pp 81−184.

(68) Walker, F. A.; Simonis, U. In *Biological Magnetic Resonance*; Berliner, L. J., Reuben, J., Eds.; Plenum Press: New York, 1993; Vol. 12 (NMR of Paramagnetic Molecules), pp 133−274.

(69) Kalodimos, C. G.; Gerothanassis, I. P.; Pierattelli, R.; Ancian, B. *Inorg. Chem.* **1999**, *38*, 4283−4293.

Table 6. ^{13}C NMR Data (δ, ppm) for $(^{13}CO)_{Fe}$ at Room Temperature[a]

solvent	$(F_8TPP)Fe^{II}-CO$	$(^5L)Fe^{II}-CO$	$(^6L)Fe^{II}-CO$	$[(^5L)Fe^{II}-CO\cdots Cu^{I}-CO]$-$(B(C_6F_5)_4)$	$[(^6L)Fe^{II}-CO\cdots Cu^{I}-CO]$-$(B(C_6F_5)_4)$
THF-d_8	206.5	206.8 (minor), 207.0	207.0, 207.1 (∼equal)	206.8 (minor), 207.4	207.0 (minor), 208.1
CD_2Cl_2	206.1	204.5	202.8, 203.6 (minor)		

[a] Characterization of $[(^{5/6}L)Fe^{II}-CO\cdots Cu^{I}]^+$ by ^{13}C NMR was not attempted.

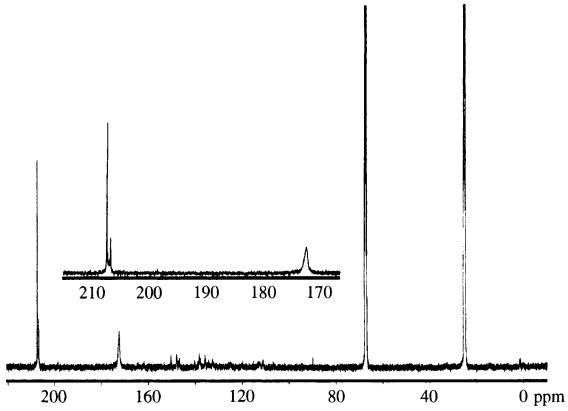

Figure 10. ^{13}C NMR spectra of $[(^5L)Fe^{II}\cdots Cu^{I}](B(C_6F_5)_4) + {}^{13}CO$ (99% enriched in ^{13}C) in THF-d_8 at room temperature. The inset shows two resonance peaks at 206.8 and 207.4 ppm, which are assigned to $(^{13}CO)_{Fe}$, and a peak at 172.4 ppm, which is assigned to $(^{13}CO)_{Cu}$. The two very intense upfield peaks (67 and 25 ppm) are due to the ^{13}C (at natural abundance) of the THF solvent.

A predominant resonance was resolved at 207.0 ppm, accompanied by a minor peak at 206.8 ppm (Figure 9). A similar spectrum was obtained for $(^6L)Fe^{II}-CO$ in THF-d_8, with the two $(^{13}CO)_{Fe}$ peaks falling at 207.0 and 207.1 ppm. However, these appear with approximately equal intensity.

The appearance of two resonances that correspond to $Fe^{II}-{}^{13}CO$ can be attributed to two different, isomeric carbonyl species in the $(^{5/6}L)Fe^{II}$ systems. We therefore assign these two peaks to isomers in which the CO is heme-bound on either the same or opposite side of the tethered TMPA, with the sixth ligand coordination site thus occupied by a THF solvent molecule or TMPA pyridyl group, respectively, as discussed previously (Chart 2). Differences in $(^{13}CO)_{Fe}$ peak ratios for the $(^5L)Fe^{II}-CO$ and $(^6L)Fe^{II}-CO$ samples might reflect the differences in heme accessibility of a solvent molecule from the same side as the TMPA group, caused by linkage at the 5-position (^5L) versus the 6-position (^6L). Table 6 lists $(^{13}CO)_{Fe}$ ^{13}C NMR resonances.

$(^{5/6}L)Fe^{II}$ carbonylation was repeated in methylene chloride-d_2 in hopes that a noncoordinating solvent would force the CO to bind below the porphyrin ring due to pyridine arm coordination above it (Chart 2). This appeared to be the case for $(^5L)Fe^{II}$ in which a single, broad peak was found at 204.5 ppm. Although the $(^6L)Fe^{II}$ sample yielded a similar broad peak at 202.8 ppm, it was accompanied by a smaller, sharp resonance at 203.6 ppm.

$[(^{5/6}L)Fe^{II}\cdots Cu^{I}](B(C_6F_5)_4)$ Carbonylation. ^{13}C NMR spectra were obtained for the Fe/Cu systems in THF-d_8 by bubbling $[(^{5/6}L)Fe^{II}\cdots Cu^{I}](B(C_6F_5)_4)$ with isotopically labeled ^{13}CO. This yielded two $(^{13}CO)_{Fe}$ peaks at 206.8 and 207.4 ppm for $[(^5L)Fe^{II}-CO\cdots Cu^{I}-CO](B(C_6F_5)_4)$, in nearly identical ratios to those found in the $(^5L)Fe^{II}-CO$ sample in THF-d_8. However, a new and comparatively broad peak emerged at 172.4 ppm that was not seen in the $(^5L)Fe^{II}-CO$ spectrum. This peak was significantly stronger in intensity than the numerous (unlabeled) ligand peaks (85−160 ppm), and so, it was attributed to a $Cu^{I}-{}^{13}CO$ resonance (Figure 10). This was confirmed by recording a ^{13}C NMR spectrum of $[(TMPA)Cu^{I}(CH_3CN)](B(C_6F_5)_4)$ in THF-d_8 after bubbling with ^{13}CO, which yielded a single, downfield shifted peak at 180.3 ppm for $(^{13}CO)_{Cu}$, similar in shape and position to that found in the Fe/Cu systems (e.g., Figure 10). See Table 7 for a list of $(^{13}CO)_{Cu}$ ^{13}C NMR resonances.

Table 7. ^{13}C NMR Data (δ, ppm) for $(^{13}CO)_{Cu}$ at Room Temperature in THF

$[(^5L)Fe^{II}-CO\cdots Cu^{I}-CO](B(C_6F_5)_4)$	$[(^6L)Fe^{II}-CO\cdots Cu^{I}-CO](B(C_6F_5)_4)$	$[(TMPA)Cu^{I}-CO](B(C_6F_5)_4)$
172.4	178.2	180.3

Conclusions

Reduced $(^{5/6}L)Fe^{II}$ and $[(^{5/6}L)Fe^{II}\cdots Cu^{I}](B(C_6F_5)_4)$ species have been isolated, characterized, and shown to have reactivity toward CO. Upon carbonylation, spectral changes have been observed in UV−vis, IR, and $^{1,2}H$ NMR spectroscopies for the $(^{5/6}L)Fe^{II}-CO$ and $[(^{5/6}L)Fe^{II}-CO\cdots Cu^{I}-CO](B(C_6F_5)_4)$ species. Unique ^{13}C NMR spectra have also been obtained for the carbonylated compounds. Results for these tethered systems have shown close agreement to those obtained for the untethered, carbonylated parent compounds $(F_8TPP)Fe^{II}-CO$ and $[(TMPA)Cu^{I}-CO](B(C_6F_5)_4)$ as well. In addition, IR studies have shown that it is possible to displace CO from the Cu of the tethered Fe/Cu compounds by addition/bubbling with Ar, yielding compounds in solution of the form $[(^{5/6}L)Fe^{II}-CO\cdots Cu^{I}](B(C_6F_5)_4)$. These monocarbonylated compounds are of special interest for future photochemical experimentation. Laser-induced flash photolysis of the heme-CO may cause intermediate binding of the photoejected CO to the copper(I), with subsequent return to the iron(II) upon relaxation. In this way, the kinetics of CO binding to the iron(II) and the copper(I) may be studied, by analogy to investigations with cytochrome *c* oxidase. Preliminary experiments with the $(^{5/6}L)Fe^{II}-CO$ compounds are currently underway.

Acknowledgment. We thank Dr. Lisa A. Marzilli and Prof. Robert J. Cotter (The Johns Hopkins University School of Medicine) for their assistance in obtaining ESI-MS data. We are grateful to the National Institutes of Health (K.D.K., Grant GM28962) for support of this research. Ryan M. Kretzer also acknowledges a Howard Hughes Summer Fellowship through the Johns Hopkins University.

IC020521I